Supporting Information

Thomsen et al. 10.1073/pnas.1306759110

SI Experimental Procedures

Purification of Proteins for Crystallography. Ligation-independent cloning was used to generate crystallography constructs in Addgene plasmid 29613 (a gift from Scott Gradia, University of California, Berkeley, CA) with N-terminal His_6 sequences and tobacco etch virus (TEV) protease cleavage site for affinity tag removal (Fig. S1*B*). Crystallography constructs were expressed in BL21 pLysS cells as described for WT caspase-3 (C3) (1, 2). Centrifuged cell pellets were resuspended in ice-cold buffer A (25 mM Tris, pH 8.0, 50 mM NaCl, 20 mM imidazole, 1 mM DTT) supplemented with 1 mM PMSF, 1 μg/mL pepstatin, and 2 μg/mL leupeptin, and clarified lysates (prepared as described earlier) were loaded onto a HisTrap HP column (GE Healthcare) using HPLC (AKTA). After washing with five to 10 column volumes of buffer A, His_6-tagged protein was eluted directly onto an in-line HiTrap Q column (GE Healthcare) using buffer B (25 mM Tris 8.0, 50 mM NaCl, 400 mM imidazole, 1 mM DTT). The Q column was washed with five to 10 column volumes of buffer B, and eluted with a 100 mL gradient to 50% buffer C (25 mM Tris, pH 8.0, 1 M NaCl, 1 mM DTT). Eluted protein was treated with TEV protease at a 20:1 (caspase:TEV) molar ratio overnight at 4 °C, and injected over a HisTrap HP column equilibrated in buffer A. Flow through was concentrated to ∼2 mL and injected onto a HiLoad 16/60 Superdex 200 prep-grade column (GE Healthcare) equilibrated in buffer D (250 mM NaCl, 25 mM Tris, pH 8.0, 1 mM DTT). The eluted protein was pooled, concentrated to 20 mg/mL, flash-frozen in liquid nitrogen, and stored at −80 °C. Selenomethionine-labeled Δ*N*-procaspase-3-C163A (Δ*N*-P3-C163A) was purified in the same manner as unlabeled protein with the following modifications. Minimal M9 media was used for selenomethionine incorporation as described, the protein was expressed for 6 h after IPTG induction, and Tris(2-carboxyethyl)phosphine at a concentration of 1 mM was used in place of DTT (3).

To prepare acetyl-Asp-Glu-Val-Asp-chloromethylketone (Ac-DEVD-CMK)-labeled procaspases for crystallography and phage selection, Δ*N*-P3-D175A and Δ*N*-procaspase-7-D198A (Δ*N*-P7-D198A) (purified as described for Δ*N*-P3-C163A) at 5 μM were labeled in a common buffer (50 mM Hepes, pH 6.5, 50 mM KCl, 0.1 mM EDTA, 1 mM DTT) by incubating with 80 μM or 40 μM of Ac-DEVD-CMK (American Peptide Company) respectively, and incubating for 1 h at 37 °C. The resulting protein solutions were run over HisTrap, HiTrap Q, and S200 columns to isolate a population of 100% labeled proenzyme and stored as described for Δ*N*-P3-C163A.

Protein Crystallization and Cryoprotection. All P3 constructs were dialyzed overnight into a solution of 10 mM Tris 8.0, 10 mM DTT, and 50 mM NaCl, and all P7 constructs were dialyzed into a solution of 10 mM Tris 8.0, 2 mM DTT, and 50 mM NaCl. P3 crystal form 1 (P3-1) was crystallized by mixing equal volumes of protein at 10 mg/mL in dialysis buffer with a solution of 10% PEG 3350 and 200 mM ammonium citrate, pH 5.0, and harvested by exchanging into a solution of 9 mM Tris, pH 8.0, 9 mM DTT, 45 mM NaCl, 25% PEG 3350, 180 mM ammonium citrate, pH 5.0, and 10% glycerol, and flash-freezing in liquid nitrogen. P3 crystal form 2 (P3-2) was crystallized by mixing equal volumes of protein at 10 mg/mL in dialysis buffer with a solution of 16% PEG 3350, 150 mM ammonium citrate, pH 4.9, 1 mM 1541 derivative (not observed in electron density), and 5% DMSO, and harvested by exchanging into a solution of 9 mM Tris, pH 8.0, 9 mM DTT, 45 mM NaCl, 25% PEG 3350, 135 mM ammonium citrate, pH 4.9, and 10% glycerol, and flash-freezing in liquid nitrogen. P3-DEVD was crystallized by mixing equal volumes of protein at 10 mg/mL in dialysis buffer with a solution of 10% PEG 3350 and 250 mM $CaCl_2$, and harvested by exchanging into a solution of 9 mM Tris, pH 8.0, 9 mM DTT, 45 mM NaCl, 25% PEG 3350, 225 mM $CaCl_2$, and 10% PEG 200, and flash-freezing in liquid nitrogen. P7-DEVD was crystallized by mixing equal volumes of protein at 10 mg/mL in dialysis buffer with a solution of 200 mM ammonium formate and 20% PEG 3350, and harvested by exchanging into a solution of 9 mM Tris, pH 8.0, 9 mM DTT, 45 mM NaCl, 25% PEG 3350, 180 mM ammonium formate, and 10% PEG 200, and flash-freezing in liquid nitrogen. Caspase-7 (C7):P7 was crystallized by mixing equal volumes of protein at 10 mg/mL in dialysis buffer with a solution of 200 mM Na/K phosphate, 100 mM Bis-Tris propane, pH 6.5, and 20% PEG 3350, and harvested by exchanging into a solution of 9 mM Tris, pH 8.0, 9 mM DTT, 45 mM NaCl, 25% PEG 3350, 180 mM Na/K phosphate, 90 mM Bis-Tris propane, pH 6.5, and 10% PEG 200, and flash-freezing in liquid nitrogen. A single C7:P7 crystal was obtained, and all follow-up screen failed to produce additional hits.

Structure Solution and Refinement. An initial solution for the P3-1 structure was obtained via molecular replacement by using a P3 homology model (SWISS-MODEL) based on the structures of P7 [Protein Data Bank (PDB) ID codes 1K88 and 1GQF] (4–6). This molecular replacement model assisted in identifying Se sites and calculating de novo single wavelength anomalous dispersion (SAD) phases by using a 3.3-Å selenomethionine dataset and an molecular replacement (MR)-SAD strategy implemented by PHENIX, giving a figure of merit (FOM) of 0.36 for unmodified phases and an FOM of 0.75 after density modification (7). These phases were extended into a 2.5-Å native dataset using PHENIX, giving an FOM of 0.62, and the initial homology model was rebuilt into these maps. The P3-2 structure was solved by using the fully refined P3-1 structure as a molecular replacement search model. The P3-DEVD structure was solved by using a high-resolution structure of mature C3 (PDB ID code 2DKO) as the search model (8). The P7-DEVD structure was solved by using a structure of mature C7 (PDB ID code 1F1J) as the search model (9). The C7:P7 structure was solved by using a structure of mature C7 (PDB ID code 1F1J) as the search model (9).

All structural models were refined by using individual atomic coordinates, group (P3-2) or individual (all others) atomic displacement parameters (B-factors), and translation libration screw (TLS) (with groups defined by the TLSMD server) (10). Simulated annealing omit maps and prime and switch maps calculated by using the AutoBuild component of Phenix were used to assist in bias removal for all molecular replacement solutions. All structures were stereochemically validated by using MolProbity (11). Structural analysis was conducted by using PyMOL (Schrödinger). Energy-minimized linear interpolations were created by using a crystallography and NMR system (CNS) script written by the Yale Morph Server, and movies were created by using PyMol (12, 13).

Biochemical Assays. Additional assays were conducted at pH 6.0, 6.5, 7.0, or 7.5 in three reported caspase buffers: buffer 1 (100 mM Hepes, 5 mM $CaCl_2$, 0.1% CHAPS, 10 mM DTT), buffer 2 (50 mM KCl, 50 mM Hepes, 0.1 mM EDTA, 0.1% CHAPS, 10 mM DTT), or buffer 3 (100 mM NaCl, 20 mM Pipes, 10% sucrose, 1 mM EDTA, 0.1% CHAPS, 10 mM DTT) (1, 2, 14). As these kinetic assays did not reach saturation under all conditions, and

displayed substrate inhibition in others, we compared the catalytic rates at a single intermediate concentration of substrate (500 μM). To ensure that trace levels of active enzyme did not dominate kinetic measurement of P3-D_3A or P7-D_2A, Ac-DEVD-CMK was added at 10% of the final enzyme concentrations in all proenzyme assays as described previously (2). For assays conducted at high (>400 μM) concentrations of Ac-DEVD-AFC, the emission wavelength was adjusted from 495 to 515 nM to prevent saturation of the detector. For antigen-binding fragment (Fab) NT5-14 and P3-D_3A kinetic assays, the two proteins were incubated in 384-well plates at the indicated concentrations in 22.5 μL assay buffer for 30 min, at which point 2.5 mL of 10× Ac-DEVD-AFC substrate (SM-Biochemical) was added, and the plate was read immediately. Nonlinear regression analyses for standard Michaelis–Menten and dose–response assays were performed in KaleidaGraph (Synergy Software).

MS. MS assays were conducted in duplicate at room temperature by using a LCT Premier liquid chromatography/electrospray ionization MS instrument (Waters). P3-D_3A and P7-D_2A were prepared in modified assay buffer 2 (lacking CHAPS detergent) at 10 μM and stored on ice. Ac-DEVD-CMK titrations were prepared as 2× stocks in modified assay buffer 2 (lacking both CHAPS and DTT) and stored on ice. Labeling reactions were initiated by mixing equal volumes of protein solution and Ac-DEVD-CMK solution. Sample mixing was offset by mass spectrometer acquisition time so that each reaction proceeded for 1 h at room temperature. Mass spectra were analyzed with MassLynx (Waters) by using the MaxEnt algorithm, and percentage labeling was estimated by integrating peak area for labeled and unlabeled protein.

Phage Display, Affinity Maturation, and Fab Characterization. For the initial selections, P3-DEVD and P7-DEVD at 10 μg/mL were adsorbed to MaxiSorp immunoassay plates (Thermo Scientific) for 2 h at room temperature. A limited diversity phage display library (gift from Sachdev Sidhu, University of Toronto, Toronto, ON, Canada) enriched for serine and tyrosine in complementarity determining regions (CDRs) was used for all selections (15, 16). In rounds 2, 3, and 4 of the selections, 100 μg/mL, 200 μg/mL, and 200 μg/mL of counterselection protein (P3, P7, C3-DEVD, or C7-DEVD) were incubated with phage solutions for 1 h before target panning. Individual clones were assayed for conformational selectivity via direct phage ELISA in 384-well format against P3, P3-DEVD, or C3-DEVD by using a SpectraMax M5 plate reader. Signal-to-noise ratios were calculated by dividing ELISA signals by those obtained against BSA negative controls. For high-throughput Fab characterization, tight binding clones exhibiting desired specificity profiles were subcloned into phagemid vectors lacking phage gene III and expressed in phosphate-depleted media as described previously (17). Expression cultures were lysed by using B-PER direct lysis reagent (Thermo Scientific), and purified by using HiTrap protein A affinity columns (GE Healthcare). Purified Fab was added at final concentrations between 2 and 10 μM to 20 μM of P3-D_3A (pretreated with 1% Ac-DEVD-CMK) in a final volume of 45 μL of assay buffer. Assays were initiated by adding 5 μL of 8 mM Ac-DEVD-AFC.

For affinity maturation of the lead antibody, soft randomization of CDR H3 and L3 was conducted as described previously (18). P3-DEVD was biotinylated by using EZ-Link Sulfo-NHS-SS-Biotin (Thermo Scientific) and incubated with streptavidin MagneSphere paramagnetic particles (Promega) as described previously (19). A Kingfisher 96 (Thermo Scientific) was then used to perform three rounds of selection in solution. Bound phage was eluted by using 20 mM Tris(2-carboxyethyl)phosphine, 40 mM Tris, pH 7.4, buffer. The resulting clones were characterized as described earlier with the exception that 5 μM purified Fab and 10 μM P3-D_3A was used for biochemical assays initiated by adding 5 μL of 2 mM Ac-DEVD-AFC. NT5-14 showed a conformationally selective response in initial binding assays by using surface plasmon resonance; however, nonspecific interactions between the surface plasmon resonance chip surface and caspase constructs, as well as difficulty in identifying surface regeneration conditions, prevented us from robustly fitting the binding data. Competition ELISAs were thus used to estimate the dissociation constants for Fab NT5-14 binding to P3 and C3 and fit by using nonlinear regression analysis in KaleidaGraph (Synergy Software) using the methods of Martineau (20) and Friguet (21).

Expression of Fabs in a Custom-Engineered *Escherichia coli* Cell Line. Genes encoding for Fabs were PCR-amplified from phage supernatants and cloned into a custom vector (pJK4) containing a Tac promoter (pTac) and an SfiI cloning cassette encoding no affinity tags. For expression of highly pure Fab, recombineering was used to knock out the genes that encode for periplasmic serine endoprotease (*degP*) and tail-specific protease (*prc*) in the isogenic strain C43 (DE3) (Lucigen) to generate the PRO (*ΔdegP Δprc ΔompT*) strain (22, 23). Recombineering was performed according to standard protocols to replace *degP* with a cassette encoding kanamycin resistance and *prc* with a cassette encoding tetracycline resistance (24). Additionally, a mutagenic oligonucleotide was used to introduce a W148R mutation in *spr* to correct the thermosensitive phenotype of *prc* KO strains and generate the PRO+ strain (23). The resulting cells (C43 PRO+) were transformed with expression plasmid, induced with 1 mM IPTG at an OD_{600} of 0.6, and expressed overnight at 30 °C. Centrifuged cells were resuspended in lysis buffer (50 mM Tris, pH 8.0, 150 mM NaCl) and clarified lysates prepared as described earlier for caspase expression. Lysate was loaded onto a HiTrap Protein A column equilibrated in buffer A (PBS solution, pH 7.4), washed with 100 mL buffer A, and eluted with buffer B (100 mM acetic acid). Eluted protein was immediately loaded onto a HiTrap S HP column (GE Healthcare) equilibrated in buffer C (50 mM sodium acetate, pH 5.0), and eluted by using a 100 mL gradient to 50% buffer D (50 mM sodium acetate, pH 5.0, 1 M NaCl). Concentrated protein solution was then run over a HiLoad 16/60 S200 prep-grade column (GE Healthcare) in buffer E (20 mM Tris, pH 7.5, 150 mM NaCl). Fab NT5-14 complexes with P3-DEVD were run on the S200 column by using buffer E supplemented with 1 mM DTT.

1. Wolan DW, Zorn JA, Gray DC, Wells JA (2009) Small-molecule activators of a proenzyme. *Science* 326(5954):853–858.
2. Zorn JA, Wolan DW, Agard NJ, Wells JA (2012) Fibrils colocalize caspase-3 with procaspase-3 to foster maturation. *J Biol Chem* 287(40):33781–33795.
3. Van Duyne GD, Standaert RF, Karplus PA, Schreiber SL, Clardy J (1993) Atomic structures of the human immunophilin FKBP-12 complexes with FK506 and rapamycin. *J Mol Biol* 229(1):105–124.
4. Riedl SJ, et al. (2001) Structural basis for the activation of human procaspase-7. *Proc Natl Acad Sci USA* 98(26):14790–14795.
5. Chai J, et al. (2001) Crystal structure of a procaspase-7 zymogen: Mechanisms of activation and substrate binding. *Cell* 107(3):399–407.
6. Arnold K, Bordoli L, Kopp J, Schwede T (2006) The SWISS-MODEL workspace: A Web-based environment for protein structure homology modelling. *Bioinformatics* 22(2):195–201.
7. Adams PD, et al. (2010) PHENIX: A comprehensive Python-based system for macromolecular structure solution. *Acta Crystallogr D Biol Crystallogr* 66(pt 2):213–221.
8. Ganesan R, Mittl PR, Jelakovic S, Grütter MG (2006) Extended substrate recognition in caspase-3 revealed by high resolution X-ray structure analysis. *J Mol Biol* 359(5):1378–1388.
9. Wei Y, et al. (2000) The structures of caspases-1, -3, -7 and -8 reveal the basis for substrate and inhibitor selectivity. *Chem Biol* 7(6):423–432.
10. Painter J, Merritt EA (2006) TLSMD Web server for the gernation of multi-group TLS models. *J Appl Cryst* 39:109–111.
11. Chen VB, et al. (2010) MolProbity: All-atom structure validation for macromolecular crystallography. *Acta Crystallogr D Biol Crystallogr* 66(pt 1):12–21.
12. Brunger AT (2007) Version 1.2 of the crystallography and NMR system. *Nat Protoc* 2(11):2728–2733.

13. Flores S, et al. (2006) The Database of Macromolecular Motions: New features added at the decade mark. *Nucleic Acids Res* 34(database issue):D296–D301.
14. Stennicke HR, Salvesen GS (1997) Biochemical characteristics of caspases-3, -6, -7, and -8. *J Biol Chem* 272(41):25719–25723.
15. Persson H, et al. (2012) CDR-H3 diversity is not required for antigen recognition by synthetic antibodies. *J Mol Biol* 425(4):803–811.
16. Fellouse FA, et al. (2007) High-throughput generation of synthetic antibodies from highly functional minimalist phage-displayed libraries. *J Mol Biol* 373(4):924–940.
17. Gao J, Sidhu SS, Wells JA (2009) Two-state selection of conformation-specific antibodies. *Proc Natl Acad Sci USA* 106(9):3071–3076.
18. Bostrom J, Lee CV, Haber L, Fuh G (2009) Improving antibody binding affinity and specificity for therapeutic development. *Methods Mol Biol* 525:353–376, xiii.
19. Rizk SS, et al. (2011) Allosteric control of ligand-binding affinity using engineered conformation-specific effector proteins. *Nat Struct Mol Biol* 18(4):437–442.
20. Martineau P (2010) Affinity measurements by competition ELISA. *Antibody Engineering*, eds Kontermann R, Dübel S (Springer, Berlin), Vol 1, pp 657–665.
21. Friguet B, Chaffotte AF, Djavadi-Ohaniance L, Goldberg ME (1985) Measurements of the true affinity constant in solution of antigen-antibody complexes by enzyme-linked immunosorbent assay. *J Immunol Methods* 77(2):305–319.
22. Ali M, et al. (2005) Improvements in the cell-free production of functional antibodies using cell extract from protease-deficient Escherichia coli mutant. *J Biosci Bioeng* 99(2):181–186.
23. Chen C, et al. (2004) High-level accumulation of a recombinant antibody fragment in the periplasm of Escherichia coli requires a triple-mutant (degP prc spr) host strain. *Biotechnol Bioeng* 85(5):463–474.
24. Sharan SK, Thomason LC, Kuznetsov SG, Court DL (2009) Recombineering: A homologous recombination-based method of genetic engineering. *Nat Protoc* 4(2): 206–223.

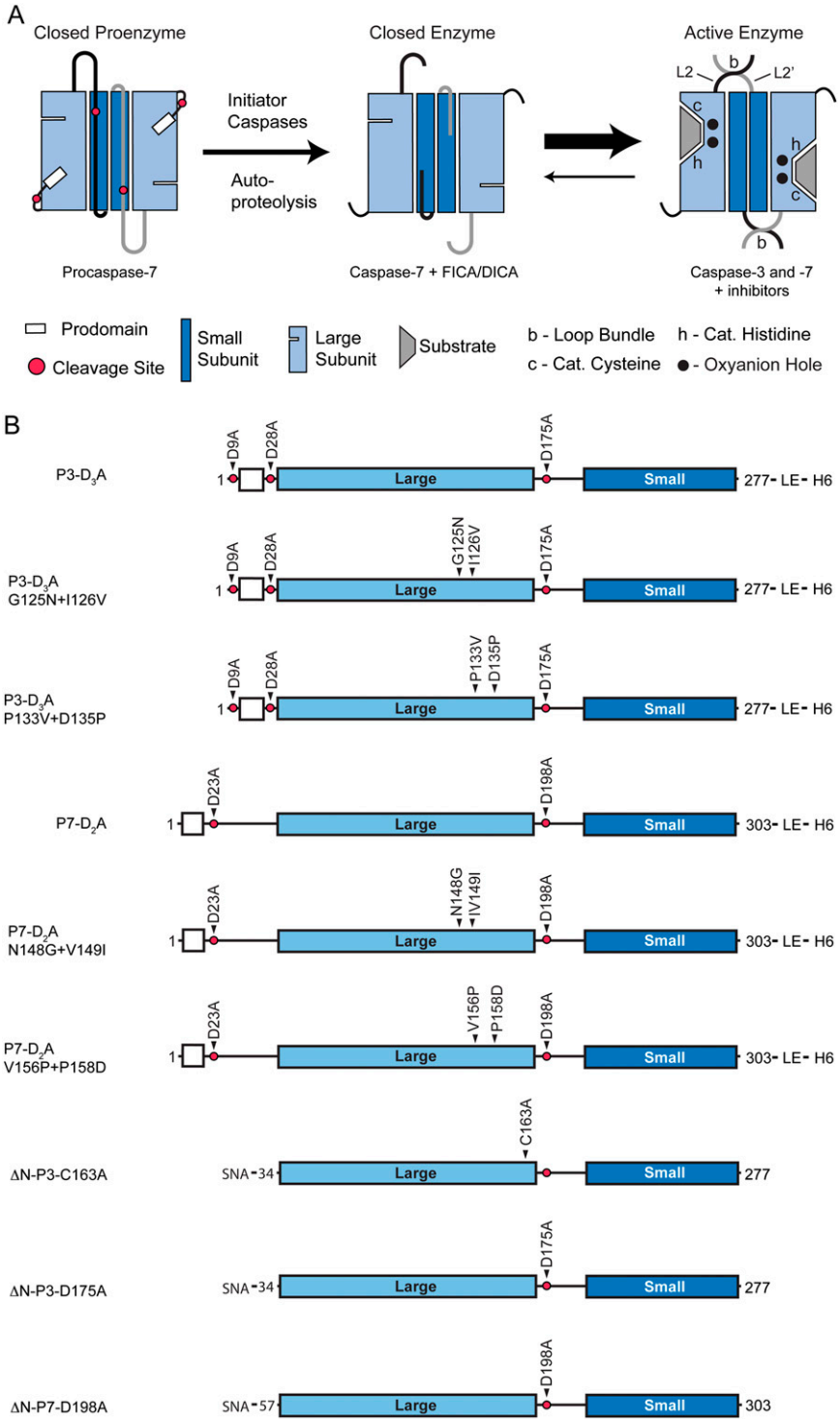

Fig. S1. Procaspase activation mechanism and protein construct design. (*A*) Proenzyme processing at caspase cleavage sites in the intersubunit linker [i.e., loop-2 (L2)] leads to formation of a loop bundle composed of L2 and L2′, which stabilizes the active conformation of the caspase in which key catalytic elements are properly positioned (see key). Structures bound to allosteric-covalent inhibitors have shown that the mature enzyme can adopt the proenzyme-like inactive conformation. Arrow size indicates relative conformational equilibrium. Diagram based on existing structural examples listed below each proposed conformational state (1–3). (*B*) A diagram of the P3 and P7 constructs used in this study with numbers corresponding to residue number and colored as in *A*. Individual mutations (i.e., D175A, corresponding to aspartate 175 mutated to alanine) are shown on the diagram with nomenclature used in the main text shown (*Left*). All single site mutants were generated by using the QuikChange site-directed mutagenesis protocol (Agilent Technologies). H6, 6× histidine tag used for affinity purification; LE, LE amino acid linker between C terminus of protein and H6 tag; SNA, SNA amino acid tag remaining after cleavage of N-terminal 6× histidine tag using TEV protease.

1. Riedl SJ, et al. (2001) Structural basis for the activation of human procaspase-7. *Proc Natl Acad Sci USA* 98(26):14790–14795.
2. Chai J, et al. (2001) Crystal structure of a procaspase-7 zymogen: Mechanisms of activation and substrate binding. *Cell* 107(3):399–407.
3. Hardy JA, Lam J, Nguyen JT, O'Brien T, Wells JA (2004) Discovery of an allosteric site in the caspases. *Proc Natl Acad Sci USA* 101(34):12461–12466.

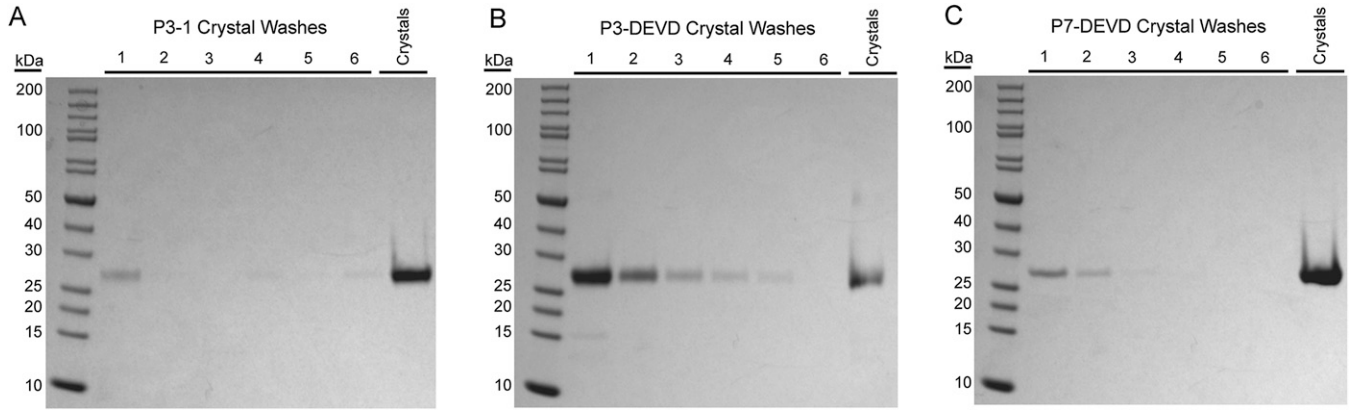

Fig. S2. Gel analysis of procaspase crystals. (*A*) Coomassie-stained reducing SDS/PAGE gel on six consecutive washes of the P3-1 crystals to remove excess protein, and on the P3-1 crystals themselves. The gel shows that the P3-1 crystals contain Δ*N*-P3-C163A at a molecular weight of ∼28 kDa, and no visible mature caspase. (*B*) Same as in *A*, but conducted on P3-DEVD crystals. Faint bands corresponding to mature C3 are visible in the first wash, but not in the crystals, which contain Δ*N*-P3-D175A labeled with Ac-DEVD-CMK at a molecular weight of ∼28 kDa. (*C*) Same as in *A*, but conducted on P7-DEVD crystals, and showing that they contain Δ*N*-P7-D198A at a molecular weight of ∼28 kDa.

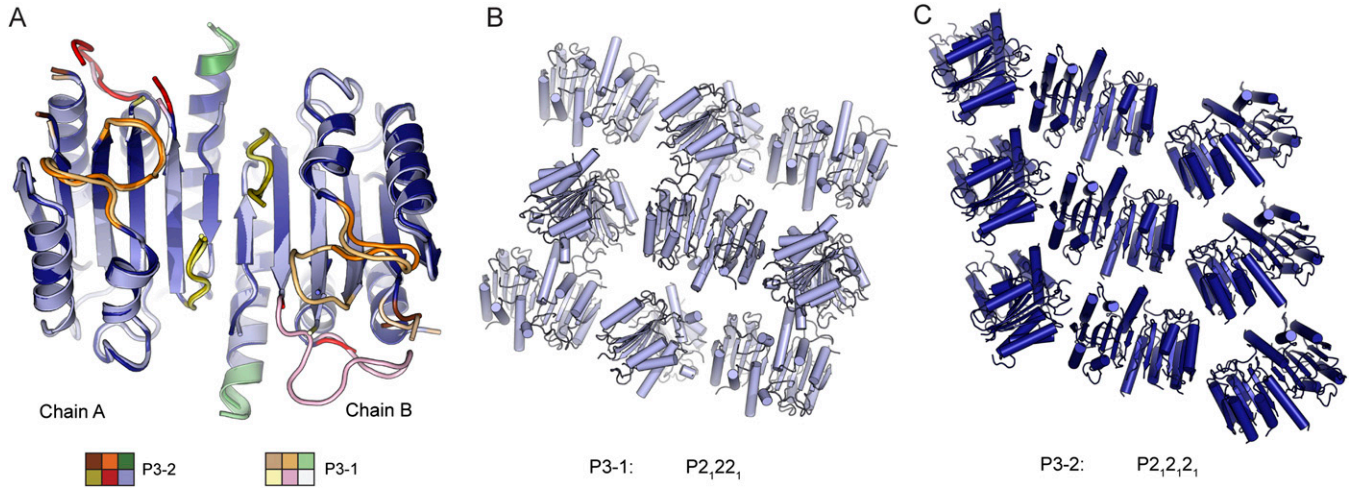

Fig. S3. Comparison of P3-1 and P3-2 crystal forms. (*A*) Structural alignment of P3-1 and P3-2. Both structures share three traits not found in P7: structural disorder and movement in loop-H (LH) that disrupts the typical β-sheet, absence of ordered density for loop-1, and winding of loop-4 into an α-helix. Additionally, both loop-3s in both structures are in the inactive conformation. Structures colored according to key and as in Fig. 1*B*. (*B*) Nine copies of the P3 dimer in the P3-1 crystal packing arrangement. (*C*) Nine copies of the P3 dimer in the P3-2 crystal packing arrangement. The central dimer is oriented as in *B*, and makes unique crystal packing contacts compared with P3-1.

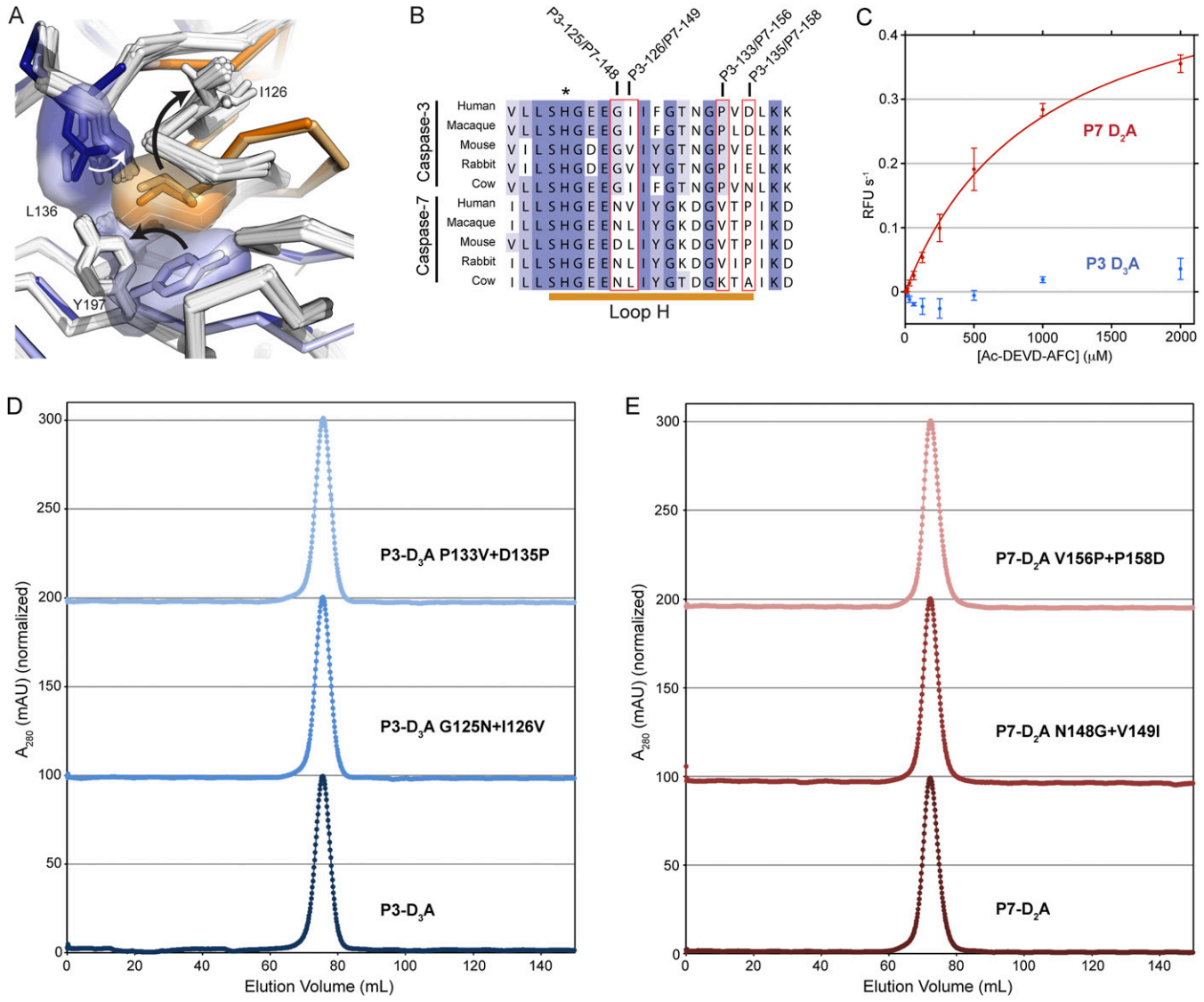

Fig. S4. Structural and functional analysis of P3 and P7. (*A*) Conformational changes in the hydrophobic core of P3 accommodate a ~180° flip of I126, which appears to stabilize the inactive LH structure. Proteins are colored according to the key in Fig. 1C. (*B*) A sequence alignment of C3 and C7 homologues in mammals showing residues in LH containing the catalytic histidine (asterisk). Changes in P3 (relative to P7) include the presence of glycine 125 adjacent to residue 126, as well as the movement of a proline at position 135 to position 133 (red boxes). These changes may alter the stability of LH, creating a metastable β-sheet structure that forms in C3, but not P3. (*C*) Although the catalytic activity of noncleavable P7 (P7 D_2A) is low (Table S2), it can be robustly measured in Ac-DEVD-AFC cleavage assays conducted in optimized C7 buffer (buffer 1) at pH 7.4. In contrast, P3 (P3 D_3A) activity in optimized C3 buffer (buffer 2) at pH 7.4 lies at or below the noise of our Ac-DEVD-AFC cleavage assay, in agreement with previous studies (1). Error bars are ± SD ($n = 3$). (*D* and *E*) HiLoad 16/60 Superdex 200 (GE Healthcare) size exclusion traces of purified P3 and P7 mutants showing that all proteins run as dimers and exhibit no aggregation. Absorbance values (*y* axis) are normalized to 100 mAU and offset by 100 mAU for different datasets.

1. Zorn JA, Wolan DW, Agard NJ, Wells JA (2012) Fibrils colocalize caspase-3 with procaspase-3 to foster maturation. *J Biol Chem* 287(40):33781–33795.

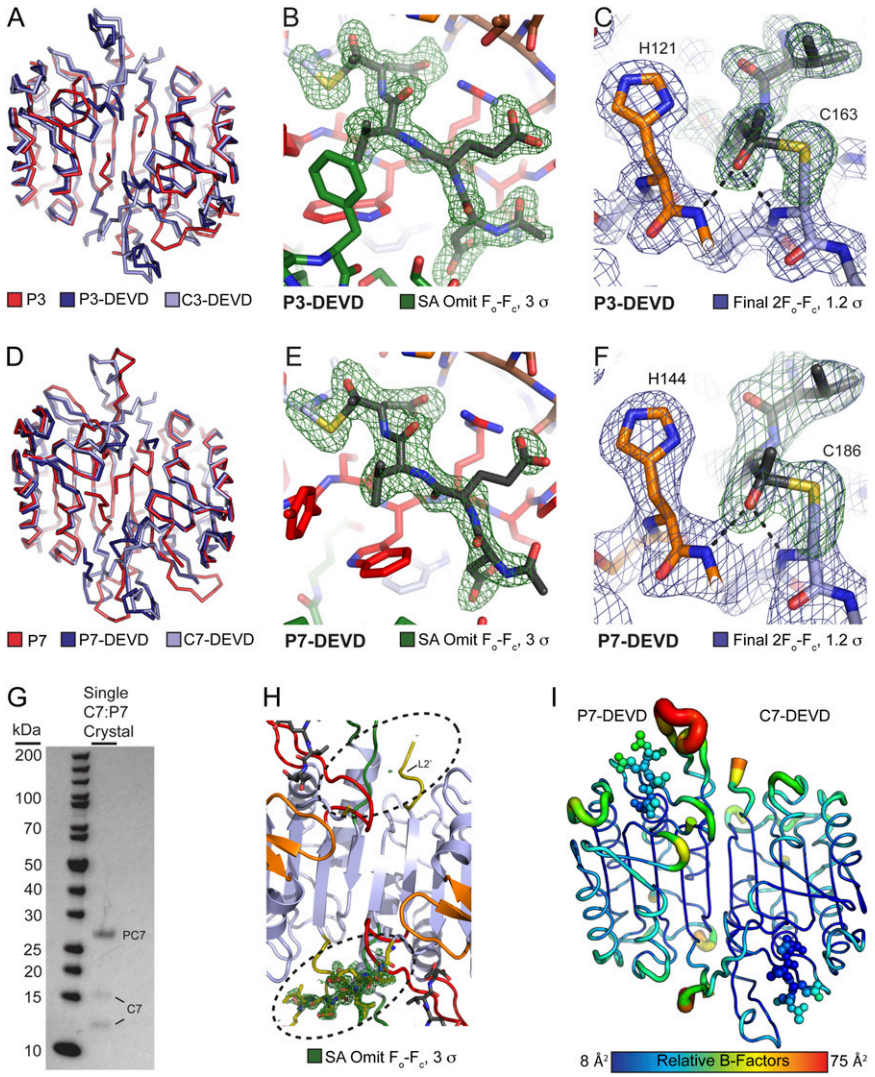

Fig. S5. Detailed analysis of P3-DEVD, P7-DEVD, and C7:P7 structures. (*A*) Overlay of P3-1, P3-DEVD, and C3-DEVD (PDB ID code 2DKO) in ribbon representation (1). P3-DEVD aligns to C3 (PDB ID code 2DKO) with a Cα rmsd of 0.8 Å and to P3-1 with a Cα rmsd of 3.3 Å across commonly resolved residues. (*B*) F_o-F_c simulated annealing omit (SA Omit) density contoured at 3σ for Ac-DEVD-CMK and the catalytic cysteine in chain A of the P3-DEVD structure. (*C*) Strong F_o-F_c simulated annealing omit and final 2F_o-F_c electron density in the 1.8-Å crystal structure supports the presence of a tetrahedral transition state intermediate in the P3-DEVD structure. Although atypical, such a conformation has been observed previously in 1.06-Å crystal structures of C3 bound to Ac-DEVD-CMK complexes (1). Dashed lines indicate that the P1 carbonyl group is within hydrogen bonding distance of the putative oxyanion hole. (*D*) Representation as in *A* for P7-DEVD. P7-DEVD aligns to C7-DEVD (PDB ID code 1F1J) with a Cα rmsd of 1.6 Å and to P7 (PDB ID code 1K88) with a Cα rmsd of 5.1 Å across all resolved residues (2, 3). (*E*) As in *B*, but for Ac-DEVD-CMK and the catalytic cysteine in chain B of the P7-DEVD structure. (*F*) As in *C*, but for Ac-DEVD-CMK and the catalytic cysteine in chain B of the P7-DEVD. Given the high degree of similarity between the P3-DEVD and P7-DEVD structures, we have modeled the bound inhibitor as a tetrahedral transition state mimic, which best fits the electron density. However, the slightly lower resolution of the P7-DEVD structure (2.15 Å) precludes a precise description of the active site geometry, and thus we cannot rule out the more typical active site arrangement in which the catalytic cysteine is bonded to the ketomethylene group of the inhibitor. (*G*) Coomassie-stained SDS/PAGE of the single crystal used for data collection. Crystal was completely exchanged into cryoprotectant before flash-freezing and data collection, after which it was run on the gel. Bands corresponding to Δ*N*-P7-D175A (P7) and mature Δ*N*-C7-D175A (C7) are shown. (*H*) SA-omit maps calculated for the areas within the dotted circles and in the absence of L2. Whereas one L2 binding site shows strong density, L2 is completely absent in the other site. (*I*) A cartoon representation of the structure colored by relative Cα B-factors, and in which thicker loops correspond to higher B-factors. Although these differences could be influenced in part by asymmetric crystal packing contacts, it is striking that the lack of L2 appears to destabilize all loops surrounding the active site.

1. Ganesan R, Mittl PR, Jelakovic S, Grütter MG (2006) Extended substrate recognition in caspase-3 revealed by high resolution X-ray structure analysis. *J Mol Biol* 359(5):1378–1388.
2. Chai J, et al. (2001) Crystal structure of a procaspase-7 zymogen: Mechanisms of activation and substrate binding. *Cell* 107(3):399–407.
3. Wei Y, et al. (2000) The structures of caspases-1, -3, -7 and -8 reveal the basis for substrate and inhibitor selectivity. *Chem Biol* 7(6):423–432.

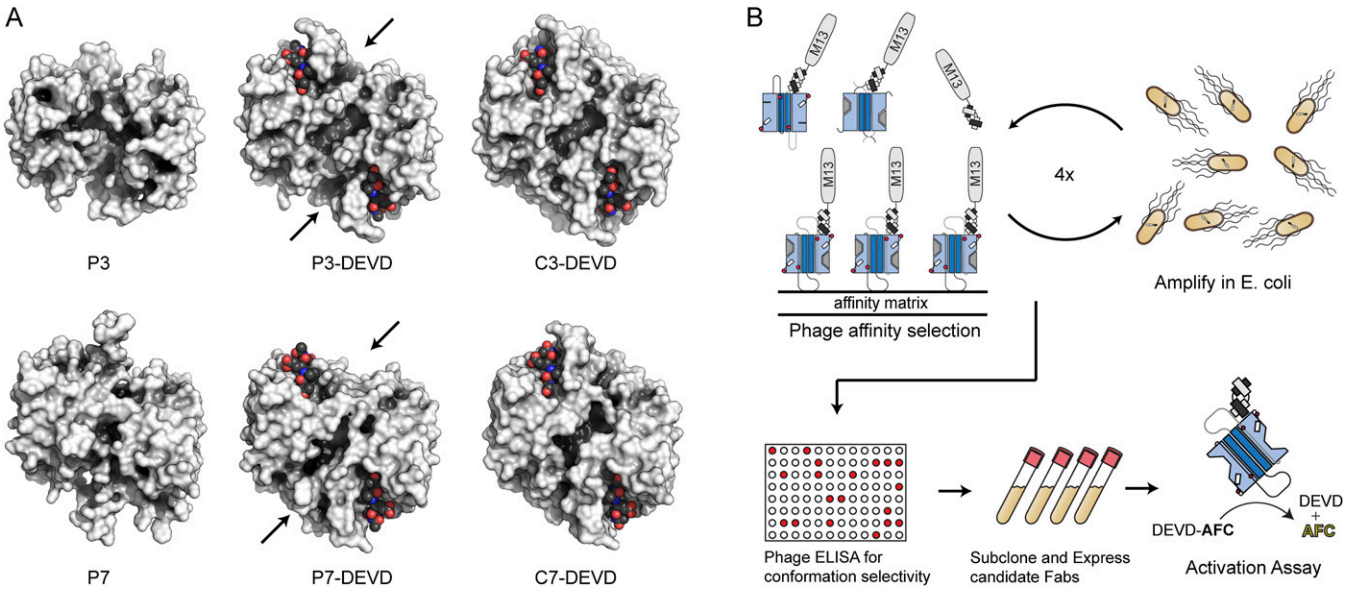

Fig. S6. Conformational selection for Fabs that bind and stabilize "active proenzymes." (*A*) Surface representations of structures reported in this paper (P3, P3-DEVD, P7-DEVD) and elsewhere revealing distinct surface features. Bound tetrapeptide substrates are shows as colored spheres. The absence of full loop bundle formation in P3-DEVD and P7-DEVD generates potential allosteric activation sites (arrows). (*B*) A diagram of the strategy for identifying conformationally selective P3-DEVD and P7-DEVD binding Fabs and characterizing their activity. Selecting only those Fabs that stimulate Ac-DEVD-AFC cleavage activity preferences allosteric activators, and helps to prevent the identification of Fabs that directly occlude the active site.

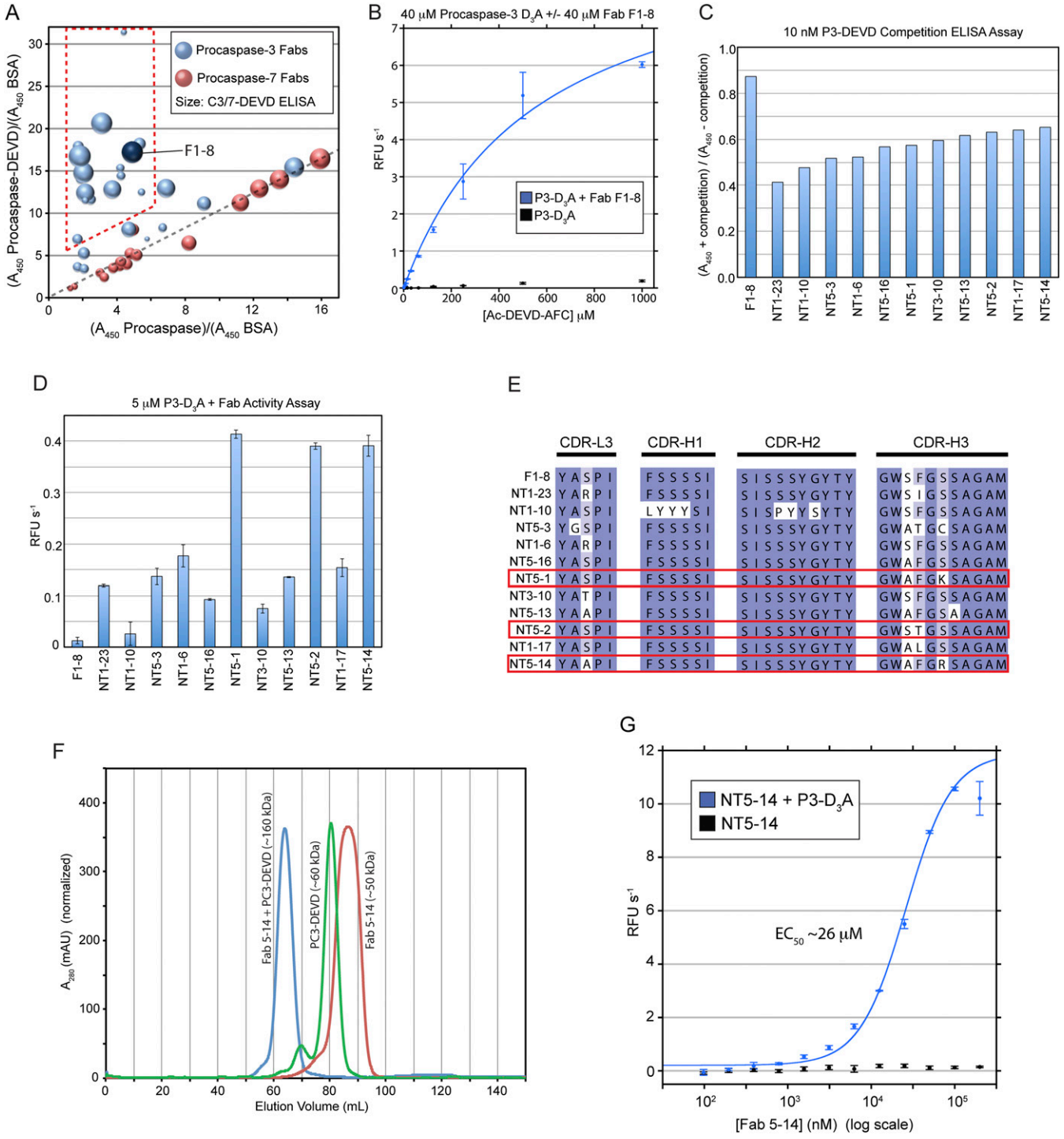

Fig. S7. Identification and characterization of a P3 stimulating Fab. (*A*) The signal-to-noise ratio in direct phage ELISAs against P3/7, P3/7-DEVD, and C3/7-DEVD shown as a bubble chart (see key). The red dashed region identifies the most desirable conformation-selective clones. The dark blue sphere corresponds to lead Fab F1-8 selected for affinity maturation. The dashed black line indicates equivalent affinity for P3 and P3-DEVD (blue spheres) or P7 and P7-DEVD (red spheres). (*B*) Kinetic analysis of 40 μM P3 D_3A in the presence and absence of an equimolar quantity of purified Fab F1-8. To prevent measurement of contaminating active C3, the irreversible covalent inhibitor Ac-DEVD-CMK was added up to 1% of the total P3 D_3A concentration (400 nM). Whereas P3-D_3A has no measurable catalytic activity alone (black), Fab F1-8 stimulates the activity of P3-D_3A (blue). Error bars represent ± SD (n = 3). (*C*) ELISA conducted on affinity-matured Fabs in the presence and absence of 10 nM P3-DEVD competition. The dissociation constant for Fab F1-8 is >>10 nM, whereas the affinity matured Fabs are much improved, with estimated dissociation constants of ~10 nM. (*D*) Ac-DEVD-AFC cleavage assays conducted on P3 D_3A in the presence of 12 P3-DEVD specific binding Fabs. All affinity-matured Fabs stimulate P3 D_3A with improved activity relative to parent Fab F1-8. Error bars represent ± SD (n = 3). (*E*) Sequence alignment of CDRs from affinity-matured Fabs compared with the parent Fab (F1-8). The three most effective Fabs from *B* are boxed in red. Background is colored from dark blue (conserved) to white (not conserved). (*F*) Size exclusion column chromatography analysis of Fab NT5-14, P3-DEVD, and the Fab NT5-14 + P3-DEVD complex. The Fab and procaspase elute at the expected volumes, and the elution volume of the complex is consistent with a 1 Fab:1 P3 stoichiometry. (*G*) A dose–response analysis of affinity matured Fab NT5-14 in the presence and absence of 5 μM P3-D_3A and 200 μM Ac-DEVD-AFC showing strong stimulation of P3.

Table S1. Data collection, phasing, and refinement statistics

Data	P3-1 SeMet	P3-1 Native	P3-2	P3-DEVD	P7-DEVD	C7:P7
Space group	$P2_122_1$	$P2_122_1$	$P2_12_12_1$	$P2_12_12_1$	$C222_1$	$P2_12_12_1$
Cell dimensions						
a, *b*, *c*; Å	54.8, 94.1, 96.2	54.6, 93.2, 95.9	50.3, 54.4, 162.0	66.0, 84.8, 96.6	57.3, 100.0, 161.6	58.5, 88.7, 88.9
α, β, γ ; °	90.0, 90.0, 90.0	90.0, 90.0, 90.0	90.0, 90.0, 90.0	90.0, 90.0, 90.0	90.0, 90.0, 90.0	90.0, 90.0, 90.0
Wavelength, Å	0.9796	1.116	1.116	1.116	1.116	1.116
Resolution, Å*	50–3.3 (3.4–3.3)	50–2.5 (2.6–2.5)	50–2.9 (3.0–2.9)	50–1.8 (1.9–1.8)	50–2.15 (2.23–2.15)	50–1.65 (1.71–1.65)
R_{sym} or R_{merge}, %*	14.4 (39.1)	10.9 (63.2)	11.4 (78.7)	5.9 (61.8)	9.2 (77.6)	5.5 (59.4)
$I/\sigma I$*	6.55 (2.21)	12.1 (1.93)	15 (1.95)	18.8 (2.2)	18.4 (1.7)	19.2 (2.1)
Completeness, %*	96.3 (98.0)	95.4 (67.3)[†]	95.1 (93.7)	99.6 (99.0)	99.8 (98.3)	99.3 (98.7)
Redundancy*	2.6 (2.5)	3.6 (3.4)	5.9 (4.8)	4.3 (3.9)	6.4 (3.8)	3.4 (3.3)
FOM[‡]	0.75	0.63				
Refinement						
Resolution, Å	—	47.9–2.50	48.0–2.89	48.3–1.80	49.7–2.15	32.87–1.65
No. reflections	—	16,766	9,982	51,020	25,641	55,899
R_{work}/R_{free}	—	20.7/24.3[§]	22.9/25.7[§]	16.3/19.5[¶]	19.7/22.7[¶]	16.1/19.7[¶]
No. atoms						
Protein	—	3,272	3,085	3,861	3,607	3,838
Ligand/ion	—	0	0	74	74	74
Water	—	48	14	429	206	386
B-factors						
Protein	—	46.4	63.5	20.7	32.5	21.1
Ligand/ion	—	0	0	22.0	47.1	18.8
Water	—	32.0	40.6	31.2	31.2	32.1
rmsd						
Bond length, Å	—	0.003	0.002	0.010	0.002	0.007
Bond angle, °	—	0.644	0.484	1.245	0.554	1.104
Ramachandran						
Preferred	—	97.6	96.9	98.0	98.0	99.1
Allowed	—	2.4	3.1	2.0	2.0	0.9
Outliers	—	0	0	0	0	0

*Values in parentheses are for highest-resolution shell.
[†]Data are >90% complete to 2.6 Å.
[‡]FOM for density modified phases.
[§]R_{free} calculated using 10% of the data omitted from refinement.
[¶]R_{free} calculated using 5% of the data omitted from refinement.

Table S2. Kinetic analysis of (pro)caspase-3 and -7

Sample	K_m, μM	k_{cat}, s^{-1}	k_{cat}/K_m, $M^{-1}{\cdot}s^{-1}$	Zymogenicity*
10 nM C7	28.0 ± 1.9	7.3 ± 0.1	2.6×10^5	NA
10 nM C3	10.8 ± 1.2	16.2 ± 0.5	1.5×10^6	NA
5 μM P7-D_2A	976 ± 86	$2.2 \times 10^{-4} \pm 9.3 \times 10^{-6}$	0.23	1,130,000
5 μM P3-D_3A[†]	ND	ND	ND	>10,000,000
5 μM P3-D_3A + 2.5 μM NT5-14	122 ± 11	$7.2 \times 10^{-4} \pm 2.6 \times 10^{-5}$	5.9	250,000
5 μM P3-D_3A + 5 μM NT5-14	112 ± 4	$1.3 \times 10^{-3} \pm 2.0 \times 10^{-5}$	11.6	130,000
5 μM P3-D_3A + 10 μM NT5-14	99.7 ± 8.3	$2.9 \times 10^{-3} \pm 8.7 \times 10^{-5}$	29.1	51,000
5 μM P3-D_3A + 25 μM NT5-14	77.0 ± 7.7	$6.0 \times 10^{-3} \pm 2.0 \times 10^{-4}$	77.9	19,000
5 μM P3-D_3A + 100 μM NT5-14	73.3 ± 7.7	$1.2 \times 10^{-2} \pm 4.3 \times 10^{-4}$	164	9,000

NA, not applicable; ND, not detectable.
*Zymogenicity is defined as the mature enzyme k_{cat}/K_m divided by the proenzyme k_{cat}/K_m.
[†]Activity of P3 is at or below the detection limit of the Ac-DEVD-AFC cleavage assay and thus no catalytic constants can be determined. Zymogenicity for P3-D_3A is thus an estimate, as reported previously (1).

1. Zorn JA, Wolan DW, Agard NJ, Wells JA (2012) Fibrils colocalize caspase-3 with procaspase-3 to foster maturation. *J Biol Chem* 287(40):33781–33795.

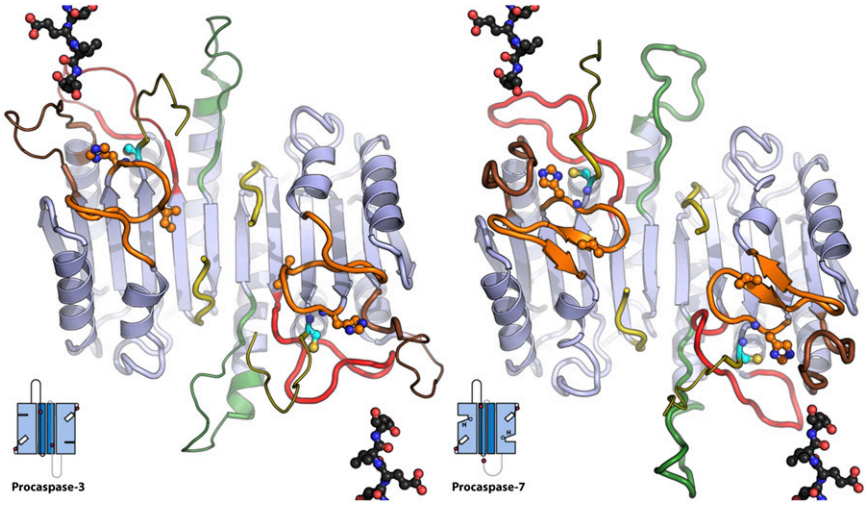

Movie S1. Conformational changes upon proenzyme maturation in P3 and P7. Energy minimized linear interpolations showing the conformational changes necessary for P3 (P3-1; *Left*) and P7 [PDB ID code 1K88, *Right*) to mature to C3 (PDB ID code 2DKO) and C7 (PDB ID code 1F1J), respectively (1–3). (*Insets*) Cartoons corresponding to structural states shown in Fig. 5. Loops are colored consistent with Fig. 1. Side chains and substrate are shown as ball-and-stick models colored by atom. Backbone nitrogen atoms defining the oxyanion hole are shown as blue spheres. Disordered residues, not visible in electron density in the procaspase structures, are modeled as thin ribbons. Typing Ctrl-L (PC) or command-L (Mac) in most media players will make the movie loop continuously.

1. Ganesan R, Mittl PR, Jelakovic S, Grütter MG (2006) Extended substrate recognition in caspase-3 revealed by high resolution X-ray structure analysis. *J Mol Biol* 359(5):1378–1388.
2. Chai J, et al. (2001) Crystal structure of a procaspase-7 zymogen: Mechanisms of activation and substrate binding. *Cell* 107(3):399–407.
3. Wei Y, et al. (2000) The structures of caspases-1, -3, -7 and -8 reveal the basis for substrate and inhibitor selectivity. *Chem Biol* 7(6):423–432.

Movie S1

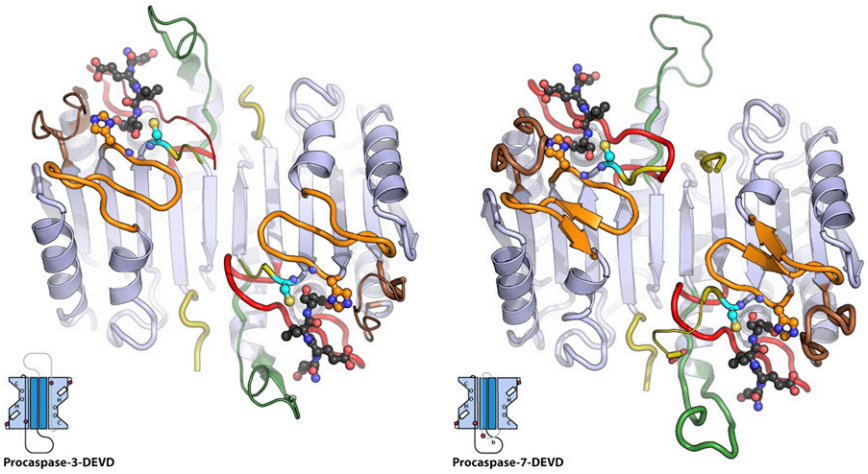

Movie S2. Conformational changes required for P3 and P7 to adopt a catalytically competent conformation in the absence of cleavage. As in Movie S1, showing interpolations between P3 (P3-1; *Left*) and P7 (PDB ID code 1K88; *Right*) to active P3 (P3-DEVD; *Left*) and active P7 (P7-DEVD; *Right*), respectively. Critical loop bundle residue, aspartate 192 in P7, is shown as sticks. Typing Ctrl-L (PC) or command-L (Mac) in most media players will make the movie loop continuously.

Movie S2